ISSN: 2578-3335 (Print) 2578-3343 (Online)

Volume 4 | Issue 1 Article 7

2022

# Establishment of an in vivo Streptozotocin-Induced Type 1 Diabetes Model Recapitulating Early Brain and Retinal Fibrosis

Kia Bourdot
*Carolinas Medical Center*, bourdotk6@rowan.edu

Lucy Dawson
*Cooper University Hospital*, lucydawson13@gmail.com

Igor Kuzin
*Cooper University Hospital*, kuzin-igor@CooperHealth.edu

Arturo Bravo Nuevo
*Philadelphia College of Osteopathic Medicine*, arturobr@pcom.edu

Zeus Antonello
*Cooper University Hospital*, antonello-zeus@cooperhealth.edu
Cooper Rowan Medical Journal: https://rdw.rowan.edu/crjcsm



## Recommended Citation

Bourdot, Kia; Dawson, Lucy; Kuzin, Igor; Bravo Nuevo, Arturo; and Antonello, Zeus (2022) "Establishment of an in vivo Streptozotocin-Induced Type 1 Diabetes Model Recapitulating Early Brain and Retinal Fibrosis," *Cooper Rowan Medical Journal*: Vol. 4: Iss. 1, Article 7.
DOI: 10.31986issn.2578.3343_vol4iss1.7
Available at: https://rdw.rowan.edu/crjcsm/vol4/iss1/7

# Establishment of an in vivo Streptozotocin-Induced Type 1 Diabetes Model Recapitulating Early Brain and Retinal Fibrosis

## Cover Page Footnote

Authors contributions: K.B., L.D., I.K., Z.A. performed experiments K.B., Z.A analyzed data, prepared figures and manuscript A.B., Z.A. designed and supervised the work This study was carried out in strict accordance with the recommendations in the Guide for the Care and Use of Laboratory Animals of the National Institutes of Health. The protocol was approved by the Institutional Animal Care and Use Committee (IACUC) of Rowan University School of Osteopathic Medicine (Protocol Number: 2017-34).

# Establishment of an in vivo Streptozotocin-Induced Type 1 Diabetes Model Recapitulating Early Brain and Retinal Fibrosis

**Kia Bourdot, MD[1]*, Lucy Dawson, B.A.Sc.[2], Igor Kuzin MD, PhD.[2], Arturo Bravo-Nuevo, PhD.[3] & Zeus Antonello, PhD.[2]**

[1]Family Medicine, Carolinas Medical Center, CHARLOTTE, NC

[2]Cooper University Hospital, Camden, NJ

[3]Philadelphia College of Osteopathic Medicine, Philadelphia, PA

*Corresponding author: bourdotk6@rowan.edu (Kia Bourdot, MD)

## ABSTRACT

INTRODUCTION: Diabetes has risen to one of the top American public health concerns. The hyperglycemic state of chronic diabetes leads to microvascular and macrovascular changes that predispose patients to delayed wound healing and organ fibrosis. The validation of models to specifically detect early, quantifiable fibrotic changes seen in the diabetic state is of fundamental importance for understanding the diabetic pathophysiology and exploring earlier management options. Here, we investigated if we could detect early signs of internal fibrosis in a streptozotocin (STZ) diabetic mouse model by quantifying α-SMA expression in various organs using flow cytometry.

METHODS: We used a low-dose STZ-induced T1DM model. T1DM was confirmed via sustained hyperglycemia (>250mg/dl) over 8-10 weeks. Delayed healing of full thickness wounds was confirmed by tracking wound healing progression over two weeks. Wounded and unwounded skin samples were analyzed histologically to quantify collagen deposition as a sign of fibrosis. Organ fibrosis was assessed in a semi-high-throughput manner using flow cytometry to quantify the percentage of alpha-Smooth Muscle Actin (α-SMA) positive cells in diabetic versus normoglycemic controls.

RESULTS: Combining STZ with post-injection glucose treatment yielded highly efficient 100% pathogenesis with 100% survival. Diabetic mice showed signs of hyperglycemia, polyuria, and delayed wound healing. Histological analysis indicated a greater increase in epidermal height and lower levels of collagen deposition in diabetic wounds. After 10-12 weeks of hyperglycemia, we observed elevated α-SMA in brain and retinal tissues.

DISCUSSION: The STZ model has previously presented cumbersome, costly, and time-intensive limitations for the study of diabetic complications. Here we tested a quantitative method for detecting early signs of fibrosis using flow cytometry. The higher percentage of α-SMA positive cells in retinal and brain tissue of diabetic mice suggests fibrosis of these tissues. We argue that this is a suitable method to study early diabetic complications.

**Keywords:** diabetes, hyperglycemia, fibrosis, murine

## INTRODUCTION

Type 1 Diabetes Mellitus (T1DM) and Type 2 Diabetes Mellitus (T2DM) have risen to one of the top American public health concerns, with a combined estimated prevalence rate of 11% (30.3 million cases) in 2015[1,2]. These numbers are predicted to rise by over 50% by 2030[1]. Although the prevalence rate of T1DM is highest among Caucasian populations, the steepest rise in incidence between 2000-2010 was seen in pediatric Hispanic populations[1–5]. Prevalence and incidence of T2DM are highest among non-Hispanic black populations[3,4]. Lower income levels and academic backgrounds are associated with higher diabetes prevalence and disease-related complications[6–9]. There is a growing need to lower the disease burden for these vulnerable populations.

Diabetes is a metabolic disorder caused by a functional insulin deficit, leading to an inability to properly absorb glucose[10]. T1DM accounts for 10% of diabetic cases. It is caused by the T-cell mediated autoimmune destruction of pancreatic islet β-cells, initiated by genetic mutation, viral infection, or environmental factors. Loss of β-cells depletes the endogenous insulin supply. T1DM is associated with autoimmune thyroid disease, celiac disease, autoimmune gastritis and Addison's disease[11]. T2DM is an acquired disorder caused by insulin resistance due to either polygenetic inheritance or metabolic overload brought on by obesity or sedentary lifestyle. Because some insulin activity is maintained, T2DM is generally a milder disease than T1DM. T2DM is associated with hypertension, dyslipidemia, metabolic syndrome, or polycystic ovarian syndrome.

In both T1DM and T2DM, hyperglycemia increases osmolarity and oxidative stress. This leads to neuropathies that impair peripheral sensation, motor control, and autonomics. Loss of functional insulin, which normally acts as a weak vasodilator, leads to increased vasoconstriction, peripheral vascular disease (PVD), and atherosclerosis of medium- and large-vessels[10]. This comorbidity of neuropathy and PVD puts patients at increased risk for chronic foot ulceration with impaired surface wound healing, which is seen in 25% of diabetic patients[12]. These ulcers often go unnoticed and become infected, which leads to increased medical costs, limb amputation, or death[12,13]. Diabetes also causes microvascular disease due the irreversible deposition of cross-linked advanced glycation end-product (AGE) proteins[14]. These AGE

proteins create space-occupying vessel obstructions, resulting in decreased perfusion, growth inhibition, apoptosis, and ultimately fibrosis of small vessels, seen in diabetic retinopathy. Diabetic hypoperfusion-induced ischemia and hyperglycemic oxidative stress also leads to increased organ fibrosis[15,16]. Fibrosis is characterized by increased extracellular matrix collagen deposition and the presence of myofibroblasts, which ultimately lead to loss of functional tissue and contraction[17,18]. Diabetic complications resulting from fibrosis include nephropathy, cardiomyopathy, coronary heart disease, stroke, nonalcoholic fatty liver disease, and pulmonary fibrosis.

Several in vivo mouse models have been used to investigate the pathophysiology of diabetes. The chemical agent streptozotocin (STZ) has been widely used to induce a type 1 diabetic state[19,20]. STZ is a toxic glucose analogue that enters pancreatic islet $\beta$-cells via Glut-2 transporter and increases reactive oxygen and nitrogen species[19,21]. This results in cell death and prohibits the biosynthesis and release of insulin, leading to sustained hyperglycemia[19,22]. STZ-induced diabetic rodents exhibit many hyperglycemic complications, including delayed wound healing, allodynia, hyperalgesia, visual impairment, renal toxicity, bradycardia, hypotension and cardiomyopathy[23,24]. However, its use to study fibrosis has been limited due to the long time-course of at least six months before the overt manifestations of fibrotic collagen depositions are apparent on histopathology[25]. Further, STZ-induced diabetes model needs to be coupled with costly genetic deficiencies to recapitulate renal fibrosis, and it requires at least six months of hyperglycemia to reproduce early signs of diabetic retinopathy, such as loss of retinal pericytes and capillaries, thickening of the vascular basement membrane, vascular occlusion and increased vascular permeability[25–29].

Extracellular matrix depositions and the appearance of myofibroblasts are thought to be hallmarks of fibrosis and wound healing across many tissues, including retinal, brain, renal, and lung samples[30–35]. Alpha-Smooth Muscle Actin ($\alpha$-SMA) is an intracellular protein expressed in these myofibroblasts that is responsible for the contractility of these cells[36]. As such, $\alpha$-SMA represents a key marker of the myofibroblastic phenotype. Nonetheless, the pathogenesis of fibrosis and appearance of myofibroblasts is complex, and $\alpha$-SMA as a fibrotic marker has been inconsistent in pulmonary, renal and muscle fibrosis[37,38]. These inconsistences could be attributed to differences in tissue properties, disease stages, experimental models or varied etiologies of the fibrotic disease[39,40].

The validation of methods and reliable markers to specifically detect early, quantifiable fibrotic changes seen in the diabetic state is of fundamental importance for understanding the diabetic pathophysiology and exploring earlier management options. Here, we investigated if we could detect early signs of internal fibrosis in an STZ-induced diabetic mouse model by measuring $\alpha$-SMA expression in various organs by flow cytometry. Flow cytometry offers unique advantages over tissue histology alone, including quick

individual cell analysis and cell sorting for further molecular studies. This method would be useful to characterize molecular and cellular changes that precede histological manifestations of fibrosis and overt disease burden seen in patients.

## METHODS

This study was carried out in strict accordance with the recommendations in the Guide for the Care and Use of Laboratory Animals of the National Institutes of Health. The protocol was approved by the Institutional Animal Care and Use Committee (IACUC) of Rowan University School of Osteopathic Medicine (Protocol Number: 2017-34). All surgery was performed under Isofluorane anesthesia, and all efforts were made to minimize suffering.

Establishment of T1DM Model: C57BL/6J male mice (The Jackson laboratories, Bar Harbor, ME) were split into normoglycemic control and hyperglycemic STZ-treated groups. At post-natal day 21 mice were injected using a low-dose streptozotocin (STZ) induction protocol (Figure 1A, B). STZ was resuspended in sodium-citrate buffer solution (pH 4.5) and injected within 10 min from preparation. Mice were injected daily intraperitoneally with 50 mg/kg STZ after fasting for 4-6 hours. STZ-driven $\beta$-cell destruction may cause severe hypoglycemia, which may be lethal. This was prevented using 10% sucrose solution for 48 hours immediately following STZ initiation[19]. Normoglycemic mice were injected with sodium-citrate buffer only. Blood glucose has been shown to peak and remain stable at three days post-STZ treatment[41]. Glycemia was checked after 5-10 days. Mice with glucose <250 mg/dL were re-injected. Hyperglycemia was sustained for 8-10 weeks prior to wounding.

Glycemia measurement: Prior to measurement, mice were food-starved for 4 hours with water ad libitum. A scalpel was used to pierce the tail and collect a drop of blood for glucose measurement using a Bayer Contour glucometer.

Wound healing model: At 8-10 weeks post-treatment, hyperglycemic and normoglycemic mice were anesthetized with isoflurane, the mouse dorsum was shaved, skin was disinfected, and two full-thickness excisional wounds were made in the anterior dorsal skin on each side of the midline with a 6 mm punch biopsy tool (Tru-Punch Sterile Disposable Biopsy Punches, Sklar Surgical Instruments, West Chester, PA). Silicon rings were custom made in house from a silicon pad (1/16 inch thick silicon sheet, Grainger, Inc.) using a 8 mm punch biopsy (Tru-Punch Sterile Disposable Biopsy Punches, Sklar Surgical Instruments, West Chester, PA) and manual cutting. This was applied with surgical glue and sutures to prevent the panniculus carnosum from closing the wound via contraction[42–45] (Figure 2A). Wound dressing (3M™ Tegaderm™) was applied after lubricating the wound with aqueous bacteriostatic gel (Surgilub, HR Pharmaceuticals, Inc., York, PA). Mice were monitored daily for 3 days for vitals and to ensure no

post-wound infections. Wounds were imaged and measured with digital calipers at 24 hours and for 3 times a week for 2 weeks.

Wound Histology: Surface wounds and matching unwounded epithelial regions from both normoglycemic and hyperglycemic mice were excised and stained for Hematoxylin and Eosin (H&E) and Masson trichrome using standard protocol (Figure 2 C, D). Samples were imaged at 50x with Leica DMi8 and DFC 7000C. Epidermal and dermal wound depth was measured with ImageJ at the maximal perpendicular height from the basement membrane. Fibrosis was quantified based on the percent of collagen present across the central 2.5 mm of the wound site, as seen on trichrome stain. Collagen was quantified using the "Colour Deconvolution" plug-in as previously described by Chen et al[46] (Figure 2E).

Tissue dissociation and flow cytometry: Whole organs, including brain, retinas, heart, lung, liver, kidney, pancreas, and peritoneal fat were collected from 8 normoglycemic and 8 hyperglycemic mice at the end of the experiment and dissociated using gentleMACS$^{TM}$ Dissociator (Miltenyi Biotec) (Figure 3A). Tissues were cut in small pieces with a scalpel and dissociated with tissue-specific programs of gentleMACS. 8 mice were used to generate 2 retina samples by pooling the retinas from 4 mice in each sample, for a total n=2 for both diabetic and non-diabetic samples. All other organs were analyzed individually, for a total n=4-8. Intracellular staining for alpha-smooth muscle actin ($\alpha$-SMA) was performed on single cell suspensions. First, cells were fixed and permeabilized using Transcription Factor Buffer Set (BD Biosciences, Jose, CA). Then cells were incubated with 2% mouse normal sera to block non-specific binding, followed by incubation with Alexa 488 conjugated anti-human $\alpha$-SMA antibodies (Invitrogen, clone 1A4). Matching isotype control was used to determine background fluorescence level. Cells were analyzed by Flow cytometry to quantify $\alpha$-SMA protein levels using S1000EX Flow cytometer (Stratedigm, San Jose, CA). Data were analyzed using CellCapture software (Stratedigm).

**RESULTS**

The T1DM model yielded highly efficient pathogenesis with 100% survival following STZ treatment with sucrose supplement. 90% of mice had sustained hyperglycemia (>250 mg/dL) at two weeks following one serial 5-day low-dose STZ treatment. The remaining 10% were given a second serial 5-day low-dose STZ treatment, after which all STZ-treated mice demonstrated sustained hyperglycemia (>250 mg/dL) (Figure 1C). Control mice injected with sodium-citrate buffer demonstrated 100% survival and normoglycemia (<150 mg/dL). Diabetic mice also demonstrated characteristic weight loss over the study period (Figure 1D). Diabetic mice demonstrated polyuria requiring more frequent cage changes (data not shown), as previously reported[47,48].

Full thickness excisional wounds with splints were photographed and measured for two weeks. A

representative image demonstrates the delay in wound healing seen grossly in diabetic mice, with measurements confirming delayed wound healing (Figure 2A, B). H&E histology stain demonstrated morphological differences in cellular architecture between unwounded and wounded tissues (Figure 2C). Unwounded tissue samples demonstrated no significant difference in dermal height in diabetic tissue compared to normoglycemic tissues, although unwounded diabetic tissues demonstrated thinner dermal height than all other samples (Figure 2F). Epidermal height for both groups was significantly increased post-injury (Figure 2G, $p<0.0001$). Diabetic wound tissues showed a larger increase in epidermal height than normoglycemic wound tissue (mean fold-change normoglycemic = 2.3; mean fold-change diabetic = 6.0). Trichrome analysis showed similar baseline collagen content in diabetic and normoglycemic unwounded tissues (Figure 2H). Post-injury, diabetic wounds demonstrated significantly impaired collagen deposition relative to normoglycemic controls ($p<0.05$).

Cell flow cytometry analysis has shown a significant increase in the percentage of α-SMA-positive cells only in brain and retinal tissues of diabetic mice compared to normoglycemic ones (Figure 3B). Although the fraction of α-SMA-positive cells did not increase in kidney and heart tissues of diabetic mice, we observed an increase in cellular levels of α-SMA expression, as demonstrated by increased α-SMA mean fluorescent intensity of these samples (data not shown). No difference was observed between normoglycemic and diabetic lung, liver, pancreas, skin, or peritoneal fat in numbers of α-SMA-positive cells or α-SMA mean fluorescent intensity.

## DISCUSSION

Given the high prevalence of diabetes and its complications, we reproduced a low-dose STZ-induced T1DM mouse model with didactic and research purposes. STZ-induced diabetes is a valuable method to study hyperglycemic complications seen in both T1DM and T2DM, including peripheral vascular disease and wound healing delay[23,24]. In the past, this model has presented cumbersome, costly, and time-intensive limitations for the study of hyperglycemic complications including pulmonary fibrosis, cardiomyopathy, retinopathy, and kidney fibrosis[25,26,49,50]. Here, we investigated if we could detect early signs of fibrosis by quantifying the number of α-SMA-positive cells across organs using flow cytometry, paired with complementary histologic analysis of surface wounds to corroborate our diabetic state.

We combined several known protocols to achieve the highest rate of diabetes induction. We successfully established a T1DM mouse model with 100% efficiency and survival, confirmed by sustained hyperglycemia, polyuria, weight loss and delayed wound closure rates compared to normoglycemic controls (Figures 1C, 1D and 2B). This is consistent with the disease manifestations seen in diabetic patients[12].

Histologic analysis demonstrated a greater increase in diabetic post-injury epidermal height than in normoglycemic tissue, indicating greater inflammation. Unwounded dermal height is smaller in diabetic mice than normoglycemic mice, but post-injury diabetic dermal height increased to match normoglycemic dermal height. Post-injury collagen deposition was decreased in diabetic mice. This is consistent with previous studies of the impaired re-epithelialization of diabetic wounds in both rat models and diabetic patients, which found that hyperglycemic tissues have altered collagen and elastin deposition[23,51,52]. These histologic findings further validate the diabetic state in our model system and offer a robust method for tracking the architectural changes that take place on a cellular scale in the hyperglycemic state.

The cellular analysis using flow cytometry demonstrated increased number of α-SMA-positive cells in the brain and eyes of diabetic mice (Figure 3B). α-SMA is a well-known marker of myofibroblasts, the cells implicated in fibrosis[30]. Diabetes is known to cause macrovascular disease by direct hyperglycemic injury to the vascular endothelium and by inhibition of nitric oxide, resulting in vasoconstriction, increased intravascular inflammation, and atherosclerosis[10]. The increase of α-SMA in brain tissue may indicate early atherosclerosis preceding diabetic stroke[53]. It is also possible this increase in α-SMA plays a role in dementia pathogenesis, although the exact mechanism for the increased prevalence of dementia among diabetic patients is unknown[54,55].

Prior studies of STZ-induced hyperglycemia have confirmed retinopathy in mice after 24-64 weeks of sustained hyperglycemia[27–29]. Here we found increased number of α-SMA-positive cells in brain and retina tissues at 10-12 weeks after hyperglycemia onset. This suggests that pro-fibrotic α-SMA-positive myofibroblasts precede the appearance of overt clinical signs. Our observation is consistent with a study that identified elevated expression of N-cadherin, α-SMA, Snail, fibronectin and connective tissue growth factor in retinal tissue purified from patients with proliferative diabetic retinopathy[29]. Our finding of elevated α-SMA expression in diabetic retinal tissues is also consistent with the fact that microvascular retinopathy is one of the earliest complications in young patients[56]. This finding is unlikely to simply be the result of STZ toxicity to retinal ganglion cells, as similar levels of retinal fibrosis have been identified across many diabetic animal model systems as well as in diabetic patient autopsies[57,58].

We were not able to confirm elevated α-SMA expression in the rest of the analyzed organs. The short diabetic disease state of 10-12 weeks at sustained hyperglycemia may be insufficient to lead to these late-stage disease complications that are often seen decades into the disease in humans. Further, although α-SMA has long been used as the standard marker for fibrosis, studies have shown that α-SMA-negative lung and kidneys are able to manifest fibrosis by other means[38,59]. Certain tissues express higher levels of alternate proteins during wound repair, such as Smad, N-cadherin, β-catenin, and Snail[15,29,30,60]. Another possible explanation for this discrepancy is that α-SMA expression may only be present in tissues that are

actively expressing fibrotic components and laying down extracellular collagen and fibrin networks[61]. After the fibrosis has taken place and collagen is laid down, α-SMA expression decreases and may not be detectable by flow cytometry. It would be useful to investigate the histology of these internal organs to visualize the extent of fibrosis.

Further analysis of organ-level diabetic fibrosis would benefit from the use of additional molecular markers to account for the variety of fibrotic response in different tissues. Flow cytometry offers a convenient method to assess the number of cells positive for a marker of interest such as α-SMA. Several cell markers could be detected simultaneously to define a pre-fibrotic profile and cascade of molecular events. For example, epithelial to mesenchymal transition (EMT) has been indicated as a process that can generate myofibroblasts and has been implicated directly in fibrosis[62]. A parallel biopsy and histologic analysis could offer complementary evidence of fibrosis and hyperglycemia-induced changes.

In summary, we successfully established the use of flow cytometry to detect early changes in the number of α-SMA positive cells in brain and retina tissue of a T1DM murine model obtained with low-dose STZ protocol. The STZ protocol is a well-known, robust and reliable method to induce diabetic hyperglycemia. We have coupled it with flow cytometry to demonstrate the feasibility of quantitative measurements of the number α-SMA-positive cells and observed changes in brain and retinal tissues. This cellular analysis is representative of increased vascular fibrosis in hyperglycemic mice central nervous system tissues, detectable as early as 10-12 weeks after hyperglycemia onset. Flow cytometry is a fast, reproducible, and reliable quantitative method that could be used to study organ fibrosis in this and other diabetic models. The quantification of cell markers involved in fibrosis could be used to investigate early events preceding diabetic retinopathy, stroke or dementia.

**References**

1. Rowley WR, Bezold C, Arikan Y, Byrne E, Krohe S. Diabetes 2030: Insights from Yesterday, Today, and Future Trends. *Population health management.* 2017;20(1):6-12.

2. Center for Disease Control. National Diabetes Statistics Report. CDC. https://www.cdc.gov/diabetes/data/statistics/statistics-report.html. Updated February 24, 2018. Accessed April 26, 2019.

3. Mayer-Davis EJ, Lawrence JM, Dabelea D, et al. Incidence Trends of Type 1 and Type 2 Diabetes among Youths, 2002-2012. *The New England journal of medicine.* 2017;376(15):1419-1429.

4. Dabelea D, Mayer-Davis EJ, Saydah S, et al. Prevalence of type 1 and type 2 diabetes among children and adolescents from 2001 to 2009. *Jama.* 2014;311(17):1778-1786.

5. Rogers MAM, Kim C, Banerjee T, Lee JM. Fluctuations in the incidence of type 1 diabetes in the United States from 2001 to 2015: a longitudinal study. *BMC medicine.* 2017;15(1):199.

6. Dagenais GR GH, Zhang X, et al. Variations in Diabetes Prevalence in Low-, Middle-, and High-Income Countries: Results From the Prospective Urban and Rural Epidemiological Study. *Diabetes care.* 2016;39:780-787.

7. Menke A, Casagrande S, Geiss L, Cowie CC. Prevalence of and Trends in Diabetes Among Adults in the United States, 1988-2012. *Jama.* 2015;314(10):1021-1029.

8. Gallup-Sharecare. State of American Well-Being: 2017 state and community rankings for the prevalence of diabetes. 2018.

9. Jordan MJ W-LL, Reels SM, et al. New Jersey Diabetes Action Plan Report. 2016.

10. Golman L, MD; Shafer, Andrew I., MD. Diabetes Mellitus. In. *Goldman-Cecil Medicine, Twenty-Fifth Edition*. 25 ed: Elsevier; 2016.

11. Tsirogianni A, Pipi E, Soufleros K. Specificity of islet cell autoantibodies and coexistence with other organ specific autoantibodies in type 1 diabetes mellitus. *Autoimmun Rev.* 2009;8(8):687-691.

12. Noor S, Zubair M, Ahmad J. Diabetic foot ulcer--A review on pathophysiology, classification and microbial etiology. *Diabetes Metab Syndr.* 2015;9(3):192-199.

13. Humphries MD, Brunson A, Li CS, Melnikow J, Romano PS. Amputation trends for patients with lower extremity ulcers due to diabetes and peripheral artery disease using statewide data. *Journal of vascular surgery.* 2016;64(6):1747-1755.e1743.

14. Cade WT. Diabetes-related microvascular and macrovascular diseases in the physical therapy setting. *Phys Ther.* 2008;88(11):1322-1335.

15. Ban CR TS. Fibrosis in diabetes complications: Pathogenic mechanisms and circulating and urinary markers. *Vascular Health and Risk Management.* 2008;4(3):575-596.

16. Yang J, Xue Q, Miao L, Cai L. Pulmonary fibrosis: a possible diabetic complication. *Diabetes Metab Res Rev.* 2011;27(4):311-317.

17. Klingberg F, Hinz B, White ES. The myofibroblast matrix: implications for tissue repair and fibrosis. *J Pathol.* 2013;229(2):298-309.

18. Hinz B, Phan SH, Thannickal VJ, et al. Recent developments in myofibroblast biology: paradigms for connective tissue remodeling. *Am J Pathol.* 2012;180(4):1340-1355.

19. Goyal SN, Reddy NM, Patil KR, et al. Challenges and issues with streptozotocin-induced diabetes - A clinically relevant animal model to understand the diabetes pathogenesis and evaluate therapeutics. *Chemico-biological interactions.* 2016;244:49-63.

20. Wu KK, Huan Y. Streptozotocin-induced diabetic models in mice and rats. *Current protocols in pharmacology.* 2008;Chapter 5:Unit 5.47.

21. Lenzen S. The mechanisms of alloxan- and streptozotocin-induced diabetes. *Diabetologia.* 2008;51(2):216-226.

22. McEvoy RC, Andersson J, Sandler S, Hellerstrom C. Multiple low-dose streptozotocin-induced diabetes in the mouse. Evidence for stimulation of a cytotoxic cellular immune response against an insulin-producing beta cell line. *J Clin Invest.* 1984;74(3):715-722.

23. Kamar SS, Abdel-Kader DH, Rashed LA. Beneficial effect of Curcumin Nanoparticles-Hydrogel on excisional skin wound healing in type-I diabetic rat: Histological and immunohistochemical studies. *Ann Anat.* 2019;222:94-102.

24. Bravo-Nuevo A, Sugimoto H, Iyer S, et al. RhoB loss prevents streptozotocin-induced diabetes and ameliorates diabetic complications in mice. *Am J Pathol.* 2011;178(1):245-252.

25. Robinson R BV, Kern TS. Update on animal models of diabetic retinopathy: from molecular approaches to mice and higher mammals. *Disease Models & Mechanisms.* 2012;5(4):444-456.

26. He X, Zhang T, Tolosa M, et al. A new, easily generated mouse model of diabetic kidney fibrosis. *Sci Rep.* 2019;9(1):12549.

27. Barriere DA, Noll C, Roussy G, et al. Combination of high-fat/high-fructose diet and low-dose streptozotocin to model long-term type-2 diabetes complications. *Sci Rep.* 2018;8(1):424.

28. Klaassen I, de Vries EW, Vogels IMC, et al. Identification of proteins associated with clinical and pathological features of proliferative diabetic retinopathy in vitreous and fibrovascular membranes. *PLoS One.* 2017;12(11):e0187304.

29. Zhou TC, D.; Lan, Y.; et al. Mesenchymal marker expression is elevated in Müller cells exposed to high glucose and in animal models of diabetic retinopathy. *Oncotarget.* 2017;8(3):4582-4594.

30. Shu DY, Lovicu FJ. Myofibroblast transdifferentiation: The dark force in ocular wound healing and fibrosis. *Prog Retin Eye Res.* 2017;60:44-65.

31. Falke LL, Gholizadeh S, Goldschmeding R, Kok RJ, Nguyen TQ. Diverse origins of the myofibroblast-implications for kidney fibrosis. *Nat Rev Nephrol.* 2015;11(4):233-244.

32. Phan SH. Genesis of the myofibroblast in lung injury and fibrosis. *Proc Am Thorac Soc.* 2012;9(3):148-152.

33. Aldrich A, Kielian T. Central nervous system fibrosis is associated with fibrocyte-like infiltrates. *Am J Pathol.* 2011;179(6):2952-2962.

34. Abu El-Asrar AM, De Hertogh G, van den Eynde K, et al. Myofibroblasts in proliferative diabetic retinopathy can originate from infiltrating fibrocytes and through endothelial-to-mesenchymal transition (EndoMT). *Exp Eye Res.* 2015;132:179-189.

35. Rocher M, Robert PY, Desmouliere A. The myofibroblast, biological activities and roles in eye repair and fibrosis. A focus on healing mechanisms in avascular cornea. *Eye (Lond).* 2020;34(2):232-240.

36. Hinz B, Celetta G, Tomasek J, Gabbiani G, Chaponnier C. Alpha-smooth muscle actin contraction upregulates fibroblast contractile activity. *Molecular Biology of the Cell.* 2001;12:2730-2741.

37. Zhao W, Wang X, Sun KH, Zhou L. alpha-smooth muscle actin is not a marker of fibrogenic cell activity in skeletal muscle fibrosis. *PLoS One.* 2018;13(1):e0191031.

38. Sun KH, Chang Y, Reed NI, Sheppard D. alpha-Smooth muscle actin is an inconsistent marker of fibroblasts responsible for force-dependent TGFbeta activation or collagen production across multiple models of organ fibrosis. *Am J Physiol Lung Cell Mol Physiol.* 2016;310(9):L824-836.

39. Usuki J, Matsuda K, Azuma A, Kudoh S, Gemma A. Sequential Analysis of Myofibroblast Differentiation and Transforming Growth factor-β1/Smad Pathway Activation in Murine Pulmonary Fibrosis. *J Nippon Med Sch.* 2012;79:46-59.

40. Wynn TA. Cellular and molecular mechanisms of fibrosis. *J Pathol.* 2008;214(2):199-210.

41. Deeds MC, Anderson JM, Armstrong AS, et al. Single dose streptozotocin-induced diabetes: considerations for study design in islet transplantation models. *Lab Anim.* 2011;45(3):131-140.

42. Chen L, Mirza R, Kwon Y, DiPietro LA, Koh TJ. The murine excisional wound model: Contraction revisited. *Wound repair and regeneration : official publication of the Wound Healing Society [and] the European Tissue Repair Society.* 2015;23(6):874-877.

43. Galiano RDM, J.; Dobryansky, M; et al. Quantitative and reproducible murine model of excisional wound healing. *Wound repair and regeneration : official publication of the Wound Healing Society [and] the European Tissue Repair Society.* 2004;12:485-492.

44. Park SA, Teixeira LB, Raghunathan VK, et al. Full-thickness splinted skin wound healing models in db/db and heterozygous mice: implications for wound healing impairment. *Wound repair and regeneration : official publication of the Wound Healing Society [and] the European Tissue Repair Society.* 2014;22(3):368-380.

45. Wang X, Ge J, Tredget EE, Wu Y. The mouse excisional wound splinting model, including applications for stem cell transplantation. *Nat Protoc.* 2013;8(2):302-309.

46. Chen YY, Qi; Xu, Cang-Bao. A convenient method for quantifying collagen fibers in atherosclerotic lesions by ImageJ software. *Int J Clin Exp Med.* 2017;10(10):14904-14910.

47. Wang-Fischer Y, Garyantes T. Improving the Reliability and Utility of Streptozotocin-Induced Rat Diabetic Model. *J Diabetes Res.* 2018;2018:8054073.

48. Fathollahi A, Daneshgari F, Hanna-Mitchell AT. Effect of Polyuria on Bladder Function in Diabetics versus Non-Diabetics: An Article Review. *Curr Urol.* 2015;8(3):119-125.

49. Russ R, Tobin B. Differential Pulmonary Vascular Effects of Streptozotocin Diabetes in Male and Female Rats. *PSEBM.* 1998;217:74-80.

50. Tate M, Prakoso D, Willis AM, et al. Characterising an Alternative Murine Model of Diabetic Cardiomyopathy. *Front Physiol.* 2019;10:1395.

51. Black E. V-PJ, Jorgensen LN. Decrease of Collagen Deposition in Wound Repair in Type 1 Diabetes Independent of Glycemic Control. *Arch Surg.* 2003;138:34-40.

52. Wang YL, K; Ledoux, WR. Histomorphological Evaluation of Diabetic and Non-Diabetic Plantar Soft Tissue. *Foot Ankle Int.* 2011;32(8):802-810.

53. Chen R, Ovbiagele B, Feng W. Diabetes and Stroke: Epidemiology, Pathophysiology, Pharmaceuticals and Outcomes. *Am J Med Sci.* 2016;351(4):380-386.

54. Cheng G, Huang C, Deng H, Wang H. Diabetes as a risk factor for dementia and mild cognitive impairment: a meta-analysis of longitudinal studies. *Intern Med J.* 2012;42(5):484-491.

55. Liu L, Li W, Zhang Y, Qin W, Lu S, Zhang Q. Weaker Functional Connectivity Strength in Patients with Type 2 Diabetes Mellitus. *Front Neurosci.* 2017;11:390.

56. Tryggestad JB, Willi SM. Complications and comorbidities of T2DM in adolescents: findings from the TODAY clinical trial. *J Diabetes Complications.* 2015;29(2):307-312.

57. Kern TS, Barber AJ. Retinal ganglion cells in diabetes. *J Physiol.* 2008;586(18):4401-4408.

58. Yang Y, Mao D, Chen X, et al. Decrease in retinal neuronal cells in streptozotocin-induced diabetic mice. *Molecular Vision.* 2012;18:1411-1420.

59. Hinz B, Phan SH, Thannickal VJ, Galli A, Bochaton-Piallat ML, Gabbiani G. The myofibroblast: one function, multiple origins. *Am J Pathol.* 2007;170(6):1807-1816.

60. Flanders KC. Smad3 as a mediator of the fibrotic response. *International journal of experimental pathology.* 2004;85(2):47-64.

61. Darby I. Alpha-smooth muscle actin is transiently expressed by myofibroblasts during experimental wound healing. *Lab Invest.* 1990;63(1):21-29.

62. Micallef L, Vedrenne N, Billet F, Coulomb B, Darby I, Desmouliere A. The myofibroblast, multiple origins for major roles in normal and pathological tissue repair. *Fibrogenesis and Tissue Repair.* 2012;5.

**Table 1 Enzyme mixture and gentleMACS$^{TM}$ Dissociator specifications for tissue processing.**

| Tissue | Enzyme (5 mL) | Media | Time |
|---|---|---|---|
| **Brain** | Trypsin EDTA | DMEM High Glucose | 15 minutes at 37 ˚C |
| **Retina** | Trypsin EDTA | DMEM High Glucose | 15 minutes at 37 ˚C |
| **Heart** | 0.15% Collagenase Type I & 0.4% BSA in PBS | DMEM High Glucose | 30 min at 37 ˚C |
| **Lung** | 0.15% Collagenase Type I & 0.4% BSA in PBS | DMEM High Glucose | 30 minutes at 37 ˚C |
| **Liver** | 0.15% Collagenase Type I & 0.4% BSA in PBS | DMEM High Glucose | 15 minutes at 37 ˚C |
| **Kidney** | 0.15% Collagenase Type I & 0.4% BSA in PBS | DMEM High Glucose | 1 hour at 37 ˚C |
| **Pan-creas** | Trypsin EDTA | DMEM High Glucose | 6-16 hours at 4 ˚C |
| **Fat** | 0.1% Collagenase Type I & 0.4% BSA in PBS | DMEM High Glucose/ M199 | 1 hour at 37 ˚C |

Figure 1

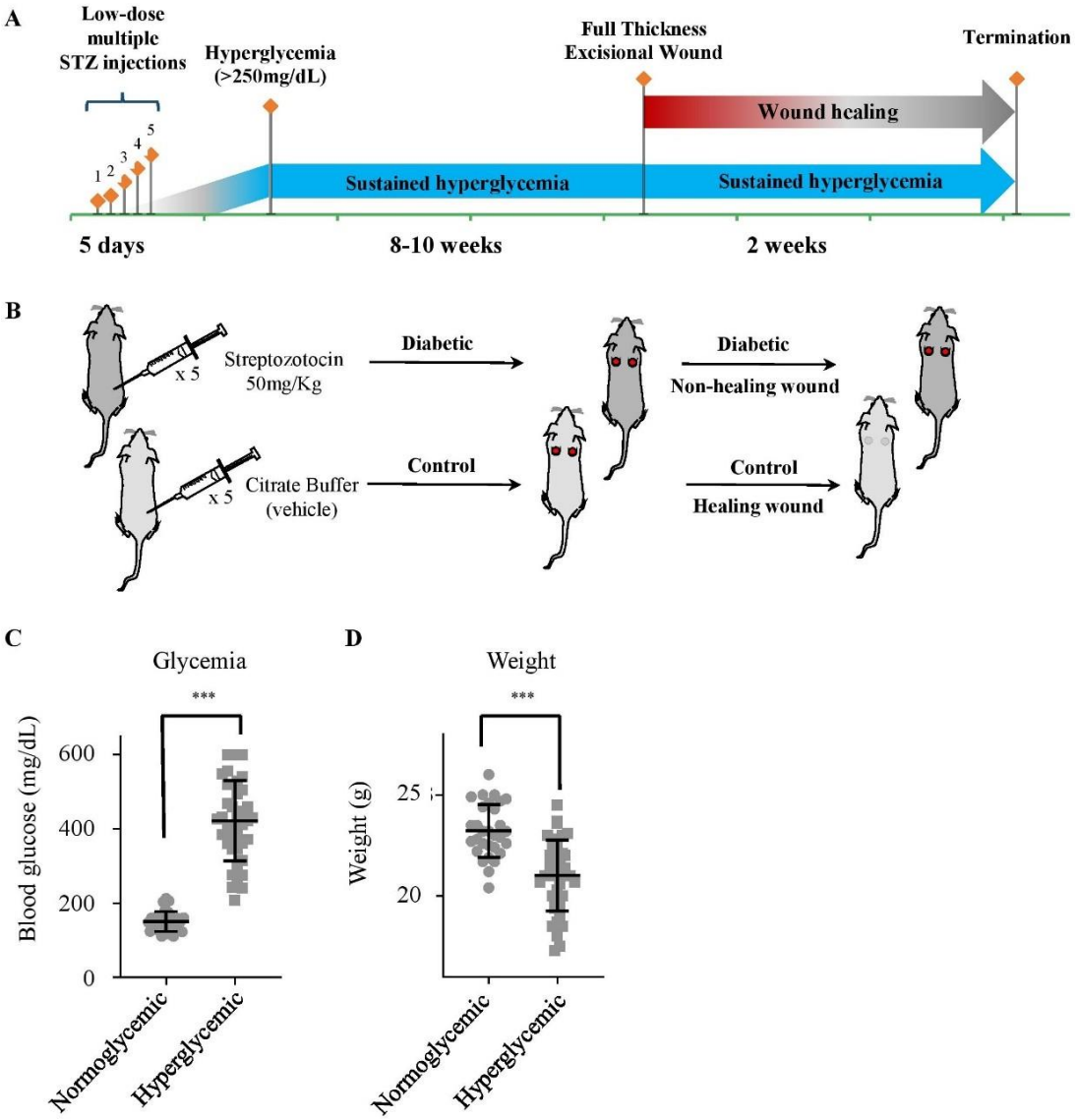


**Figure 1 Hyperglycemic wound healing murine model.** (A) Schedule for STZ injections, blood glucose monitoring, full thickness wound, healing, and termination. Histology slides and flow cytometry specimen were prepared at termination. (B) STZ was used to induce hyperglycemic diabetic state (blood glucose >250 mg/dL), and citrate buffer was injected to maintain normoglycemic control (blood glucose <250 mg/dL). STZ injections yielded 100% survival. 90% of STZ-treated mice demonstrated hyperglycemia after one treatment regimen, and 100% demonstrated hyperglycemia after a second treatment regimen. (C) STZ-treated mice demonstrated sustained hyperglycemia, confirmed prior to wounds (student's t-test, $p<0.0001$, normoglycemic n=30; hyperglycemic n=40). (D) STZ-treated mice demonstrated sustained weight loss, confirmed prior to wounds (student's t-test, $p<0.0001$, normoglycemic n=30; hyperglycemic n=40).

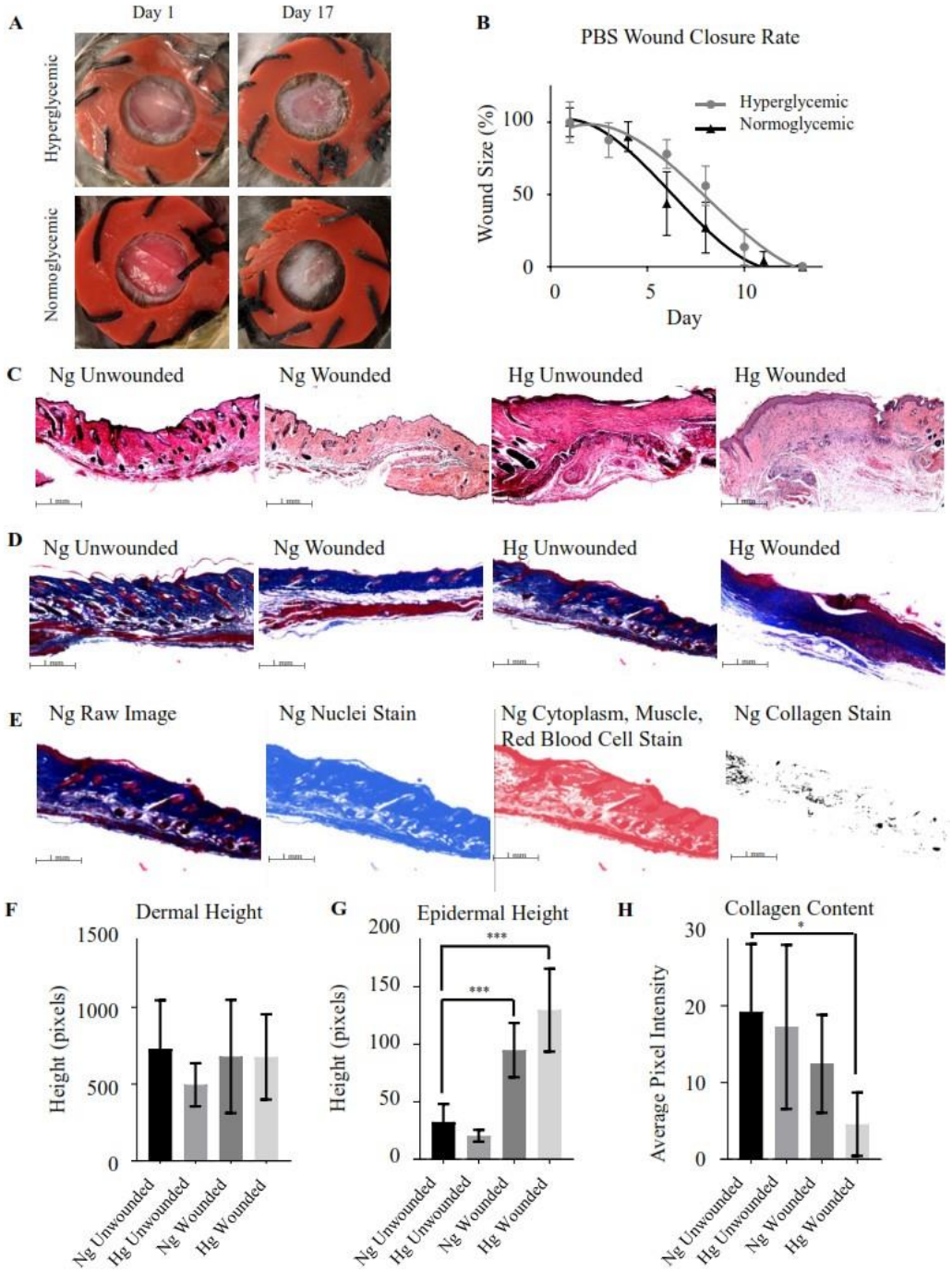


**Figure 2: Wound healing analysis of dorsal skinfold at control and wound sites.** (A) Gross imaging of splinted wounds at day 1 and 17 post-injury. (B) Gross measurement of wound closure over time demonstrates delayed closure in hyperglycemic mice. Error bars indicate standard deviation. (C) H&E stain of normoglycemic (Ng) and hyperglycemic (Hg) unwounded and wounded dorsal skin. (D) Masson-Trichrome stain of normoglycemic and hyperglycemic unwounded and wounded dorsal skin. (E) ImageJ Color Deconvolution image processing of normoglycemic G8-treated wound tissue Trichrome stain to isolate collagen stain. (F) Baseline dermal height was decreased in unwounded hyperglycemic mice compared to normoglycemic controls, although not statistically significant. Post-injury, no difference is seen in dermal height of normoglycemic and hyperglycemic tissue. Data was analyzed using unpaired 2-tailed student t-test. Ng unwounded and wounded n=16; Hg unwounded and wounded n=14. (G) Post-injury, epidermal height was significantly increased in both normoglycemic and hyperglycemic mice ($P<0.0001$). The fold-increase of unwounded to wounded epidermal height was larger in hyperglycemic mice (normoglycemic = 2.3, hyperglycemic = 6.0). Data was analyzed using unpaired 2-tail student t-test. Ng unwounded and wounded n=16; Hg unwounded and wounded n=14. (H) Decreased collagen deposition was seen in hyperglycemic wounds compared to unwounded normoglycemic tissue ($P<0.05$). Data was analyzed using unpaired 2-tail student t-test. Ng unwounded and wounded n=15; Hg unwounded and wounded n=14.

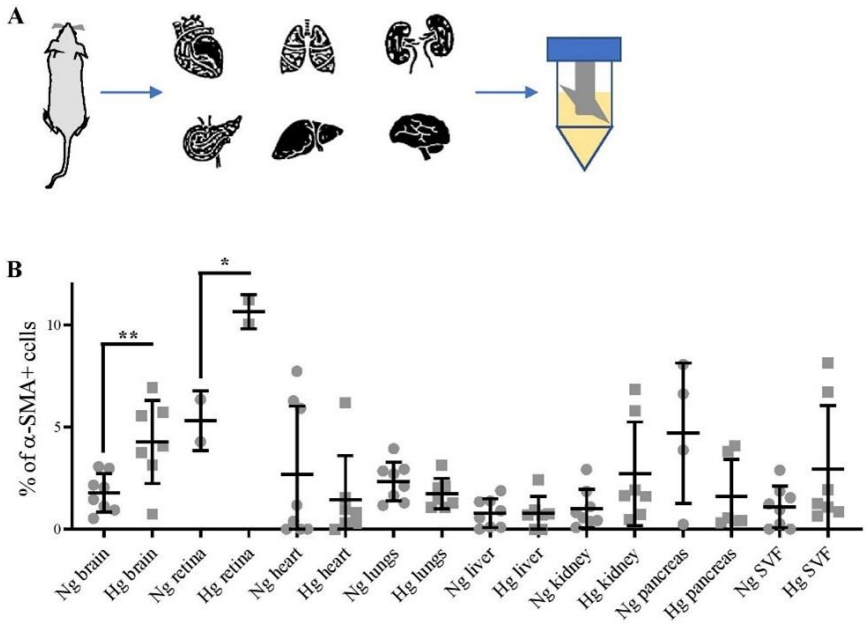


**Figure 3 Flow cytometry analysis of internal fibrosis.**(A) Mice were dissected to isolate brain, heart, lung, liver, kidney, pancreas, skin, peritoneal fat, and retinal tissue. Organs were digested using gentleMACS$^{TM}$ Dissociator at the specifications listed in Table 1 to procure cell suspension. (B) Flow cytometry data analysis of normoglycemic (Ng) and hyperglycemic (Hg) tissues revealed increased total of $\alpha$-SMA-positive cells in hyperglycemic retinas and brain ($P<0.01$) (unpaired 2-tail t-test). No difference was seen between normoglycemic and hyperglycemic lung, liver, pancreas, skin, or peritoneal fat. N=4-8 as shown, retina n=2.